

PRESSURE DROP IN A WATER FLOW THROUGH THE BOTTOM NOZZLE OF A NUCLEAR FUEL ELEMENT

Moysés Alberto Navarro, navarro@cdtn.br

Brazilian Nuclear Energy Commission (CNEN/CDTN), Belo Horizonte, 30123-979, Minas Gerais, Brazil

André A. Campagnole dos Santos, acampagnole@yahoo.com.br

Geraldo A. Campolina França, gacf@ufmg.br

Federal University of Minas Gerais, (UFMG/DEMEC), Belo Horizonte, 31270-901, Minas Gerais, Brazil

Abstract. *The characteristics of the flow through the bottom nozzle of a nuclear fuel element were analysed with a commercial CFD code, CFX 10.0. The numerical simulation was performed with an optimized mesh and three different turbulence models, $k-\varepsilon$, $k-\omega$ and SST, in a square flow channel with a standard bottom nozzle. The numerical results were compared with results of an experimental investigation accomplished to determine the pressure drop through the bottom nozzle in different water flow rates. The agreement between the numerical simulations, especially those performed with the $k-\varepsilon$ and SST turbulence models, and experimental results can be considered satisfactory. The results suggest also further numerical investigations with the piece without the geometric and boundary condition simplifications. Other turbulence models, including the LES methodology, should also be appraised for this complex geometry.*

Keywords: *nuclear fuel assembly, pressure drop, CFD, turbulence models*

1. INTRODUCTION

The end nozzles of a nuclear fuel element consist of perforated plates in which the extremities of the guide tubes of the control rods are fastened. Together with the spacer grids, this skeleton constitutes a structure that holds the rod bundle at nodes in a regular array. Beside the structural function, the plate of the bottom nozzle (BN) works as a filter, retaining debris larger than its holes. The understanding of the turbulent flow details in nuclear fuel elements is of major interest to the nuclear power industry for safe and reliable operation. Experimental studies in this complex geometry were carried out in the past, but due to the high costs associated to the experiments and difficulties of detailed measurements, the numerical approach has been pursued using computational fluid dynamics (CFD) methods (Scheuerer *et al.*, 2005). Many turbulent flow studies have been performed in a bare rod bundle (Baglietto and Ninokata, 2005, Házi, 2005), spacer grids (Anglart *et al.*, 1997, Ikeno *et al.*, 2006, Campbell *et al.*, 2005) and on perforated plates (Liu *et al.*, 2004, Frattolillo and Massarotti, 2002). However, the entrance area of the fuel element has been receiving less attention.

The objective of this study is to assess the performance of different Reynolds Averaged Navier-Stokes (RANS) turbulence models in the prediction of the turbulent flow through the standard BN of a nuclear fuel element. The numerical simulation was performed with the commercial CFD code, CFX 10.0 (2005). A mesh independence study was conducted to guarantee better numerical results. The numerical results were compared with an experimental investigation accomplished to determine the pressure drop through the BN.

2. EXPERIMENTS

Figure 1 shows the schematic diagram of the experimental apparatus used in the measurement of pressure loss through the BN. The standard BN and details of its perforated plate are also shown in Fig. 1. The experiments were performed with a water flow in a 0.23 x 0.23 x 1.41 m square duct. The uncertainty in the width of the duct was not evaluated but from the construction project it could reach up to +0.75 mm. As the width of the BN is 0.2295 m, the gap between the BN and the wall of the channel could reach up to 0.625 mm. A flow conditioner constituted of a tube bundle and a screen in its upper extremity was positioned downstream of the test section. All the signals from the pressure transmitters and thermocouples were conducted to a Data Acquisition System to “on line” monitoring and recording. The evaluated uncertainties on the measurements of the pressure drop at the positions shown in Fig. 1 were about 1% of the value. The flow conditions established in the experiment were:

- Flow rate: 115.08 ± 1.15 kg/s
- Pressure: 3.54 ± 0.04 bar
- Temperature: 55.9 ± 1.1 °C

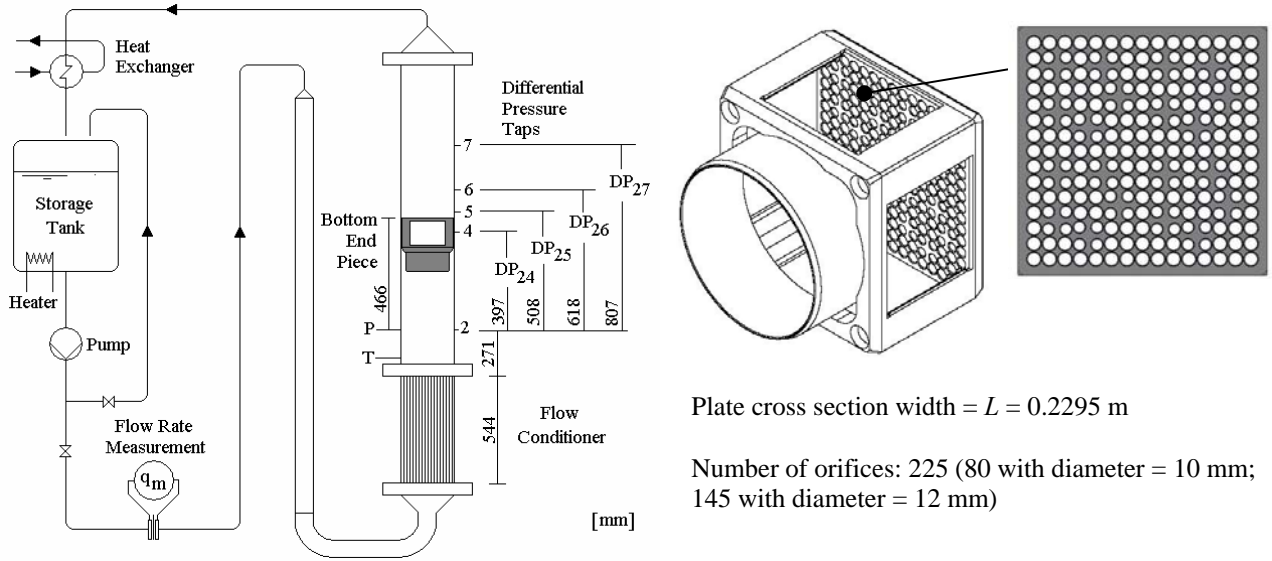


Figure 1. Experimental apparatus and BN.

3. NUMERICAL METHODOLOGY

The numerical modeling was performed using the commercial CFD code, CFX 10.0 (2005). Aiming to optimize the mesh for the BN simulation, a mesh independence study was performed splitting the BN in two separate geometries: the perforated plate and the bottom support. Splitting the geometry of the BN was necessary due to the extreme computational effort and processing time required for the BN's simulation. A large number of simulations were performed on both geometries applying different mesh configurations to obtain a mesh independent result. All of the simulations on the mesh independence study were performed within a square duct under the experimental flow condition applying the Reynolds Averaged Navier-Stokes (RANS) turbulence model $k-\epsilon$.

The mesh parameters defined for the perforated plate and bottom support in the mesh independence study were applied to the BN. Simulations were performed under the experimental flow condition described in section 2, using different RANS turbulence models. Obtained results were compared to the experimental results.

3.1. Model definition

The simulations were performed in a square channel with the dimensions: 0.2295 x 0.2295 x 1.41 m. To simulate the BN some geometrical simplifications were necessary due to mesh and numerical issues. Figure 2 shows the geometric simplifications assumed for the BN. The simplifications were basically the removal of the bevel in the external corners and the reduction of the flow duct width from 0.23 m to the same width of the BN 0.2295 m. Both simplifications had the objective to reduce the mesh size and numerical convergence issues. The four positioning orifices were also eliminated in the numerical simulations. In the simulation of the BN, the axial zero position of flow in the Z direction is the upper face of the BN's perforated plate. The x and y axis are parallel to the flow channel faces.

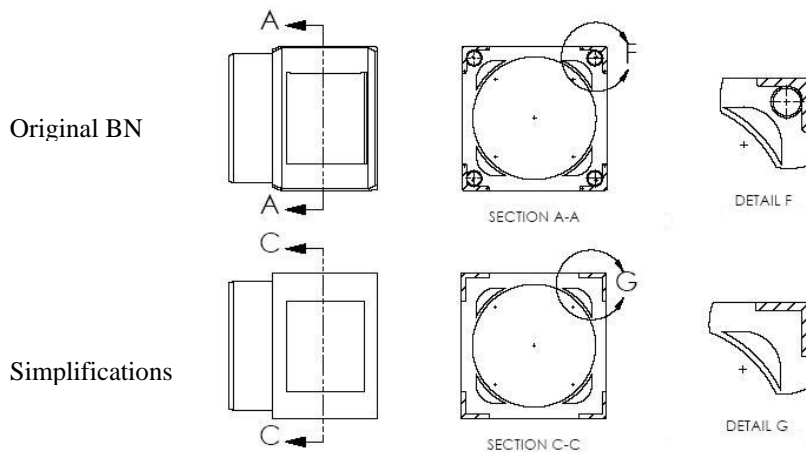


Figure 2. Simplifications in the BN geometry.

3.2. Boundary conditions

The simulations with the BN were performed under experimental conditions presented in the previous section. In this simulation, the flow rate was reduced proportionally to the flow area reduction from the experimental flow duct (0.23 x 0.23 m) to the numerical simulation model (0.2295 x 0.2295 m).

It was observed in previous simulations that the velocity profile at the inlet of the test section was almost uniform due to the presence of a flow conditioner, so an uniform profile was assumed and a 1/8 symmetry was adopted for the simulation of the BN, as shown in Fig. 3. These artifices were necessary to reduce drastically the mesh size to enable the simulation with our computational capacity. The surfaces of the duct and plate were considered smooth and the inlet turbulence intensity was assumed to be 5% (although simulations made showed no significant influence on the pressure drop when values of 1 and 10% of turbulence intensity were applied). No thermal model was used since the experiments were considered adiabatic and isothermal.

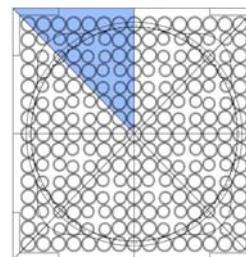


Figure 3. Symmetry planes.

3.3. Turbulence modeling and numerical scheme

Three turbulence models of two equations which fall into the category defined as eddy viscosity models were used: the $k-\epsilon$ model, developed by Launder and Spalding (1974) the $k-\omega$ model, conceived originally by Kolmogorov (1942) and reformulated by Wilcox (2000); and the Shear Stress Transport (SST) model, formulated by Menter (1994).

The $k-\epsilon$ turbulence model assumes that the turbulence viscosity is related to the turbulence kinetic energy and dissipation. In CFX the $k-\epsilon$ model uses a scalable wall-function approach to improve the near wall treatment which is made with the log-wall function. The basic idea behind the scalable wall function is to limit a lower value for the dimensionless distance from the wall used in the log-law in such a way that all the mesh points are outside the viscous sub layer. In this way all fine mesh inconsistencies near the wall can be avoided.

The $k-\omega$ turbulence model assumes that the turbulence viscosity is linked to the turbulence kinetic energy and the specific dissipation rate. In CFX the automatic wall treatment is used. The automatic wall function uses two equations, a linear equation for the viscous sub-layer and a log-law equation. Both equations are weighed in a manner that if the first node of the mesh is within the viscous sub-layer the velocity is defined more by the linear equation, if it is out, the velocity is defined more by the log-law.

In the Shear Stress Transport (SST) model the turbulent viscosity is modified to account for the transport of the turbulent shear stress. The model uses a function to blend the accurate near the surface $k-\omega$ model and the $k-\epsilon$ formulation in the outer region. This model uses the same automatic near wall treatment used in the $k-\omega$ model.

The numerical schemes applied for the simulations were a second-order central differenced scheme for the diffusion terms and a high resolution (formally second-order) upwind scheme for the convective terms. The high resolution scheme developed by Barth and Jespersen (1989) reduces numerical diffusion and dispersion by evaluating the scheme locally applying the highest order possible, between first and second-order, which does not violate the boundedness principles.

3.4. Mesh definition

In the CFX-Mesh the algorithms *Delaunay Mesher* and *Advancing Front Mesher* were used to generate the surface and the volumetric mesh, respectively. The global mesh scaling adopted in all simulations was of 16.5 mm. To reduce computational effort, a mesh independence study was carried out separately on a perforated plate and on the bottom support of the BN.

The bottom support of the BN consists of a tube of 195 mm of inner diameter, connected to square section plate of the same side length as the BN. The plate contains four small half-moon openings near the tube. The plate is connected to four angle-irons. This geometry can be seen in Fig. 4.

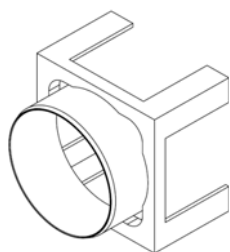


Figure 4. Bottom support.

Two localized refinements were optimized for the bottom support mesh. A refinement plane was specified on the bottom support with an influence extension equal to the support's length, 215 mm, and an element expansion factor of 1.2. A local refinement point was also defined on the small half-moon opening on the plate with the same expansion factor of 1.2 and influence extension limited to the opening. Figure 5 shows the velocity and turbulence intensity (I) profiles for the different edge length / plate hydraulic diameter (l / d_o) ratios used on both plane and point refinement. Figure 5 shows the velocity and turbulence intensity profiles 10 mm before the end of the bottom support. It can be observed that the results are very similar for the combination ratios of 0.11 for the plane refinement and 0.05 or lower for the point refinement.

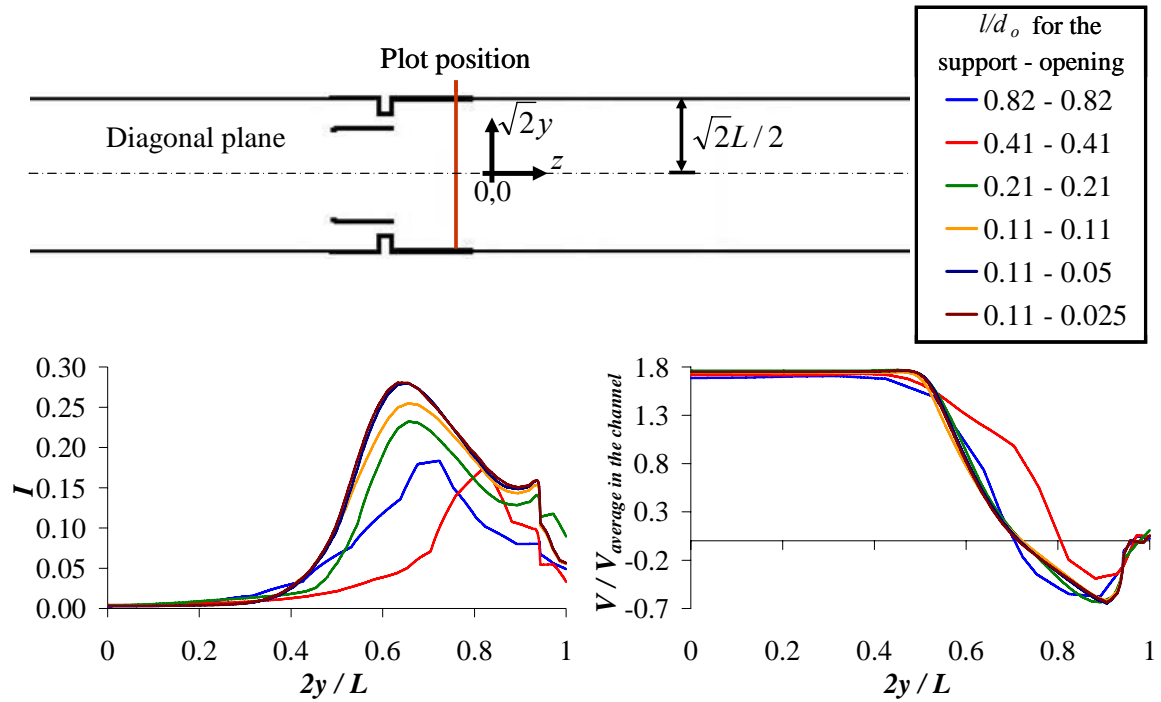


Figure 5. Velocity and turbulence intensity (I) profiles 10 mm at the end of the bottom support.

The mesh independence study of the perforated plate geometry was carried out on a perforated plate with 81 uniformly distributed orifices. The free flow area and the thickness of the perforated plate were the same of the BN. This much simpler plate was used to reduce the computational effort of the simulations. A refinement plane was specified at the plate with an influence extension equal to the plate's thickness, 20 mm, and a smooth element expansion factor of 1.1. A refinement plane was also specified after the plate where a rapid pressure recovery occurs. This second plane had an influence length equal to 13 orifice diameters and an element expansion factor of 1.2. Figure 6 shows the velocity and turbulence intensity profiles obtained in the central orifice of the plate for the different edge length / orifice average hydraulic diameter (l/d_o) ratios used in the simulations for the refinement plane on the plate. Figure 7 compares the static pressure along the channel obtained with different l/d_o ratios for the refined plane after the plate. The pressure used as reference, P_{ref} , is the experimental static pressure at tap position 2. Considering the available computational capacity the values of 0.052 for the refined plane on the plate and 0.12 for the refined plane after the plate showed a satisfactory mesh edge length.

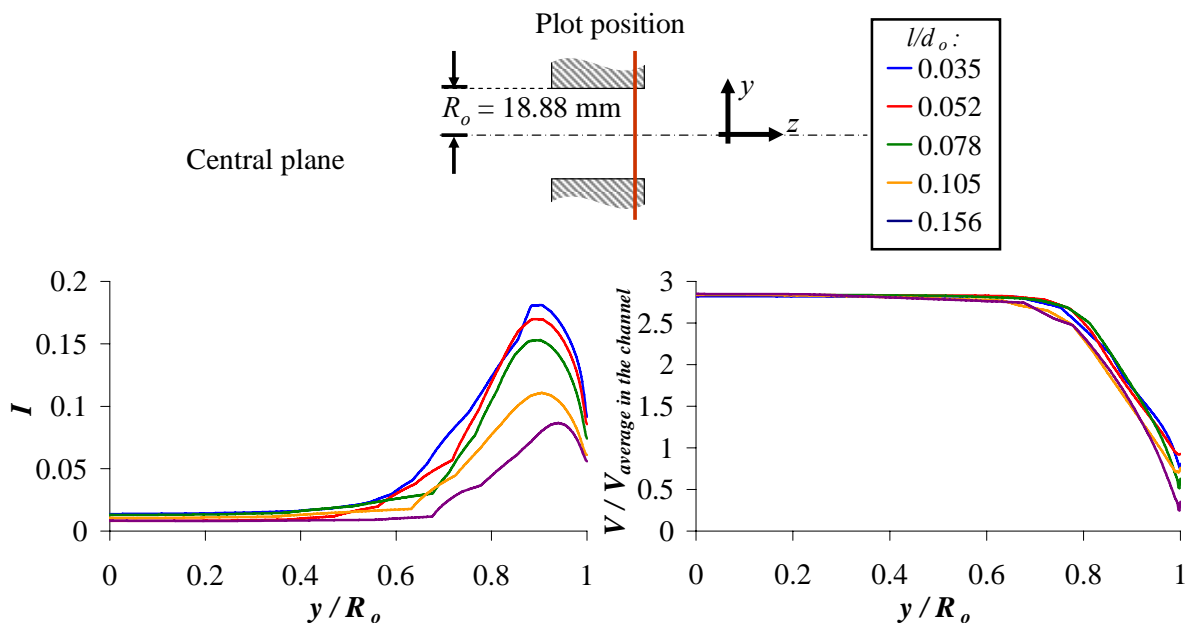


Figure 6. Velocity and turbulence intensity profiles at the exit of the perforated plate.

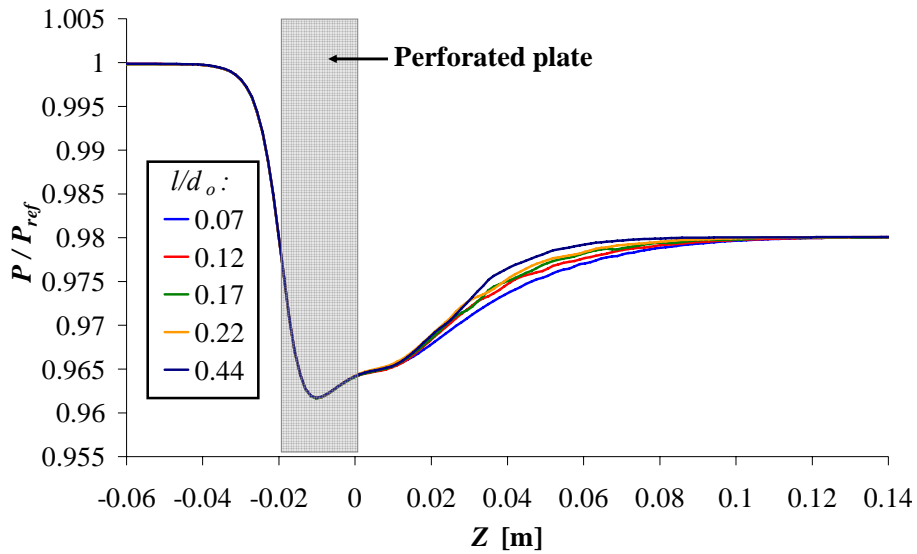


Figure 7. Pressure behavior along the channel for different mesh refinements after the perforated plate.

Near the walls, layers of structured mesh were used to capture the effects of the boundary layer in all simulations. An effort was made to maintain the value of the first dimensionless wall parameter (y^+) less than 2. This allows the $k-\omega$ and SST models to take advantage of the automatic near wall treatment. Few inconsistencies due to over refinement should be caused by the near wall mesh for the $k-\epsilon$ model, since this model uses the scalable wall function. Twenty layers were used with an expansion factor of 1.2.

Applying the defined parameter to the geometry of the BN generates the final mesh with 11681095 elements, shown in Fig. 8. All simulations were performed through parallel runs on two Pentium 4 HT PCs with 4 GB of RAM memory. The simulations took an average of 15 hours to reach an RMS convergence residual of 1×10^{-4} .

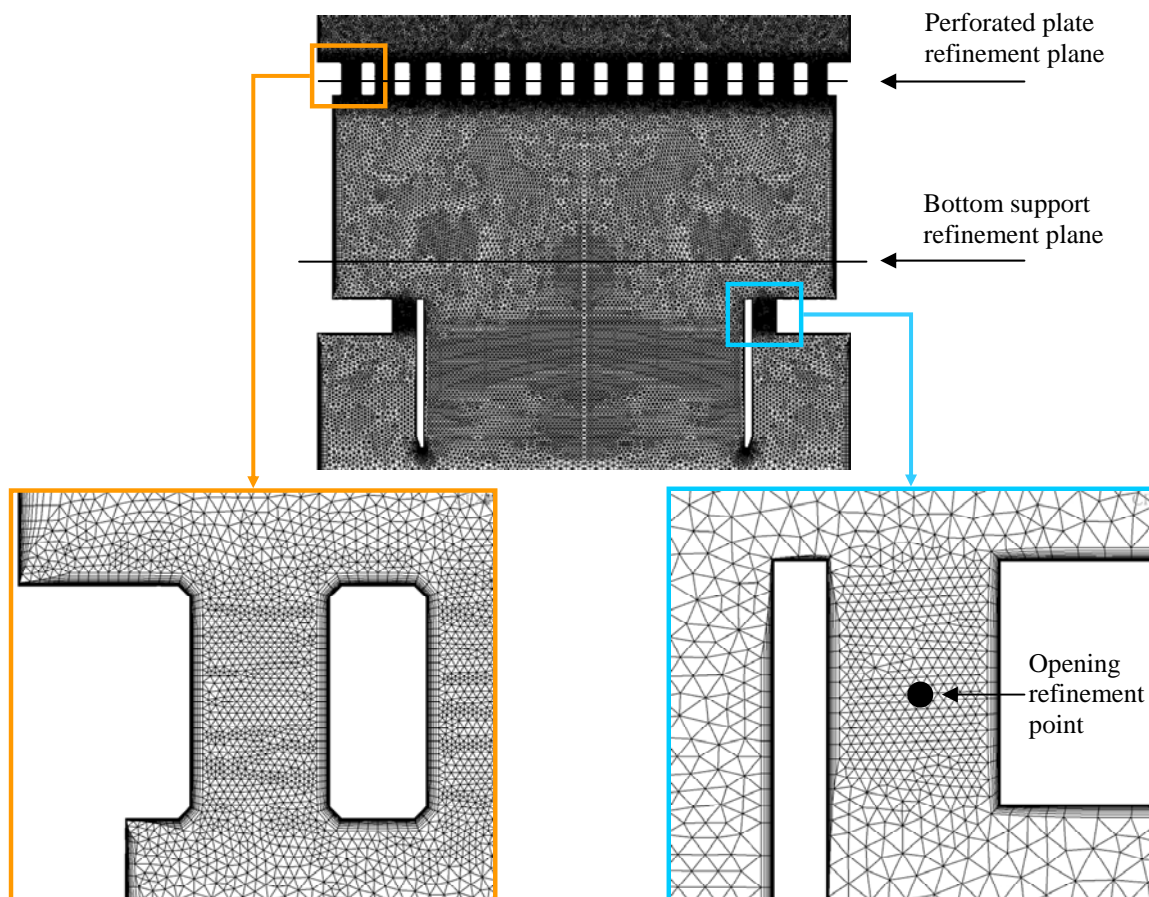


Figure 8. Details of the mesh in the region of the plate of the BN.

4. RESULTS

Figure 9 compares the experimental and numerical results of the static pressure along the flow duct with different turbulence models. The pressure used as reference, P_{ref} , is the experimental static pressure. The numerical data presented in Fig. 9 were extracted over the central line of the simulated channel.

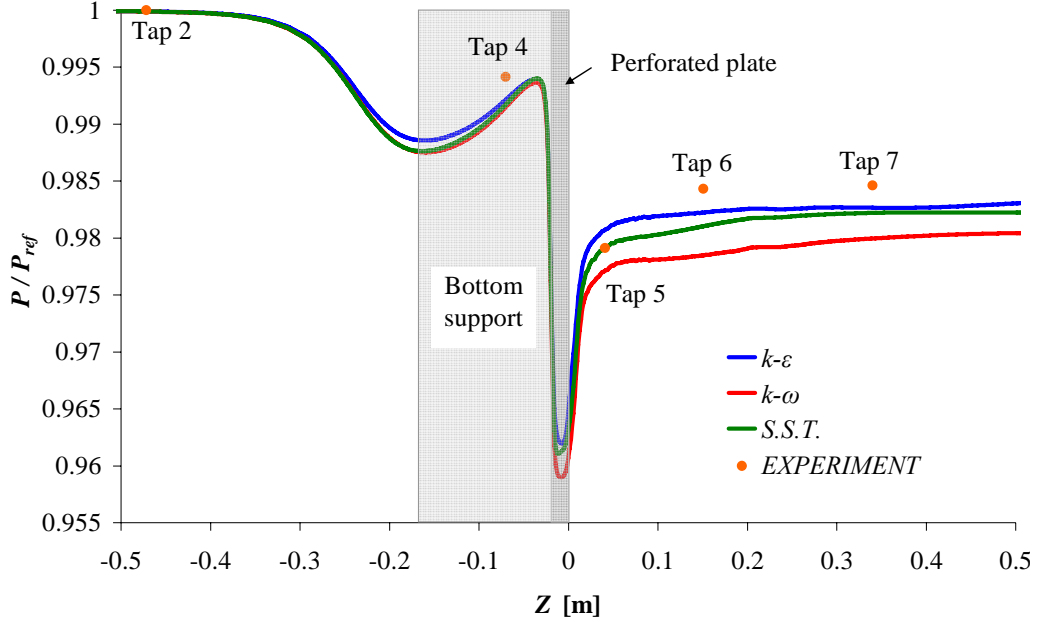


Figure 9. Pressure behavior along the channel for the experimental flow condition.

As can be observed in Fig. 9 the $k-\epsilon$ turbulence model predicts a lower pressure drop in the bottom support and in the perforated plate than the in other models. Moreover, the results obtained for the $k-\epsilon$ model are closer to those obtained in the experiment. Other observation is that most of the pressure loss occurs due to the perforated plate. The pressure loss difference observed between the simulated turbulence models, at tap position 7, is approximately the same as observed at the plate, meaning that the flow recuperation downstream of the plate has little influence on the pressure loss for all simulated models. Table 1 shows the differences of pressure drop between the tap position 2 and the remaining tap positions for the CFX calculations, performed with the three turbulence models, and the experimental results. The numerical data used to calculate the values of Tab. 1 are the average pressure extracted from a plane, normal to the flow, located at the tap positions.

Table 1. Pressure drop differences between the experimental and numerical results

| Tap | Pressure drop differences [%] | | |
|-----|-------------------------------|------------|-------|
| | Turbulence Models | | |
| | $k-\epsilon$ | $k-\omega$ | SST |
| 2-4 | 72.5 | 93.8 | 85.1 |
| 2-5 | -6.7 | 14.1 | 3.9 |
| 2-6 | 13.7 | 37.6 | 21.1 |
| 2-7 | 14.0 | 31.4 | 15.8 |

At Tab. 1 a high discrepancy between the experimental and numerical results at tap positions 2-4 for all turbulence models is observed, showing that with the mesh used in this region none of the tested models were able to accurately predict the turbulent flow. The pressure drops between the tap positions 2 and 7, away from the BN, calculated with the $k-\epsilon$ and SST models are very similar. On the whole, the pressure drops obtained with the $k-\omega$ model are higher than the ones obtained with the other models and more distant from the experimental results.

The non-dimensional velocity profiles for the simulations of the BN with the three turbulence models at the experimental tap positions are shown in Fig. 10. The profiles were obtained extracting the numerical results over a line normal to the flow direction plotted on the central plane of the flow channel. At tap positions 4 and 5, the $k-\omega$ model

predicts a recirculation near the wall larger than that predicted by the other models. At tap positions 4 and 6, the *SST* model predicts a higher velocity at the proximity of the wall of the channel than the other models.

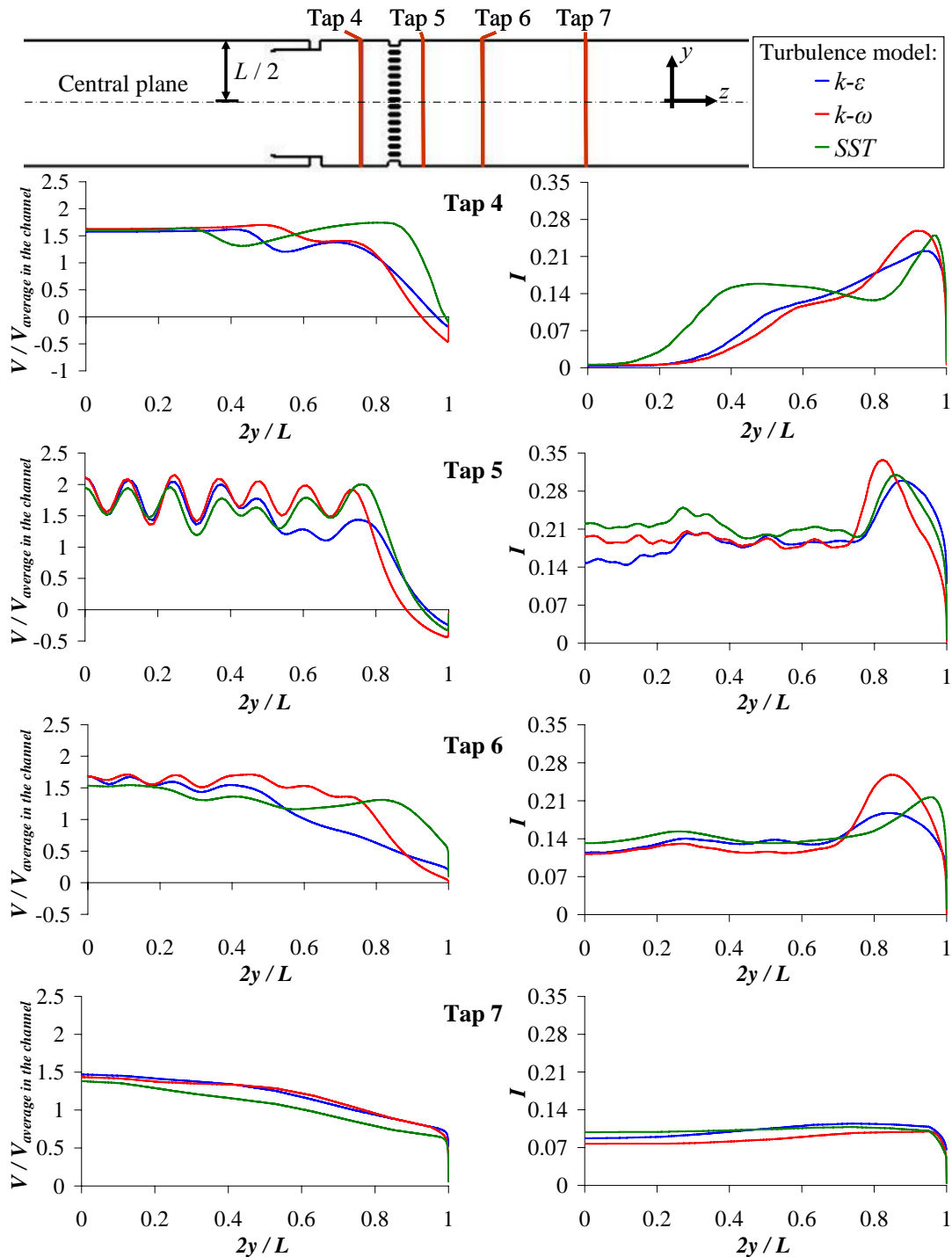


Figure 10. Velocity and turbulent intensity profiles on pressure tap positions for different turbulence models.

Figure 10 also shows the turbulence intensity (*I*) profiles for the three turbulence models on the same pressure tap positions. The profiles were obtained in the same manner as described in the previous paragraph. All three models predicted peaks of turbulence intensity at the proximity of the wall of the channel. At tap position 4, the *SST* model predicts a much larger intensity near the core of the flow compared to the other models. Figure 10 shows that at Tap position 7 neither velocity nor turbulent profiles are fully developed.

Figure 11 compares the velocity contours on the diagonal plane of the BN for all three simulated turbulence models. It can be seen that the *k-ω* model predicts a much larger recirculation near the wall downstream of the BN than the other turbulence models simulated. The *SST* model, that blends *k-ω* model near the wall to *k-ε* model in the core of the flow,

predicts a larger and more intense recirculation than that predicted by the $k-\varepsilon$ model at the bottom support region and downstream of the BN. The SST model also predicts larger recirculation at the bottom support region than the $k-\omega$ model.

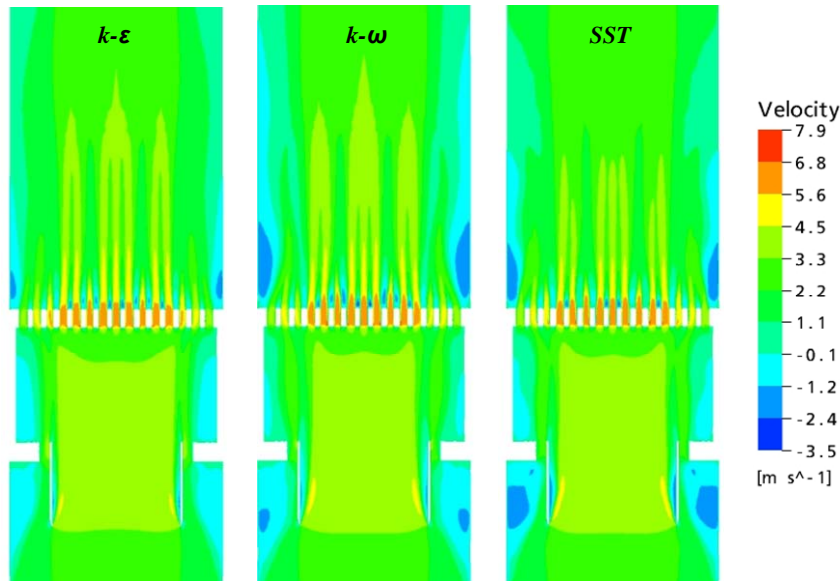


Figure 11. Velocity contours on the diagonal plane of the BN for three turbulence models.

As most of the pressure loss is due to the perforated plate this region requires special attention. Figure 12 highlights the differences between the behaviors of the flow in the perforated plate region showing the velocity contours in the direction of the flow for the simulated turbulence models. The $k-\varepsilon$ model that uses a scalable log-law near wall treatment, does not predict a recirculation of fluid after the chamfer of the orifice as is predicted by the other models that use automatic wall treatment. In the chamfer region it is also shown that the $k-\varepsilon$ and $k-\omega$ model predict a high fluid velocity near the wall.

Figure 13 shows the near wall non-dimensional velocity profiles at three positions (Fig. 12) of the central orifice. At 1 mm position, exact end of the chamfer, there is a peak of velocity near the wall that is more pronounced for the $k-\varepsilon$ and $k-\omega$ models. The fluid recirculation predicted after the chamfer, at 2 and 3 mm positions, is greater for SST than for $k-\omega$ model and is not predicted at all by the $k-\varepsilon$ model.

It is also observed in Fig. 13 that for all simulated turbulence models the central orifice shows a greater core fluid velocity than the average fluid velocity through the perforated plate. This is due to the tube of the bottom support that drives most of the fluid through the more central orifices.

Near wall results show that the influence of the wall treatment is considerable on the pressure drop and flow characteristics. The wall shear stress is an important variable for the evaluation of pressure loss due to friction. The average values predicted in the simulations for the wall shear stress were 132 Pa for the $k-\varepsilon$ model, 235 Pa for the $k-\omega$ model and 219 Pa for the SST model showing that a greater stress and therefore friction pressure loss is predicted for the models that use the automatic wall treatment. Further studies applying no wall treatment and more complex turbulence models such as LES (Large Eddy Simulation) are required to reach better understanding of the flow characteristics for this complex geometry.

The differences observed between experimental and numerical results can be attributed to several factors. One main difficulty encountered in the simulation is the presence of a gap between the BN and the channel in the experimental assembly. This gap could reach up to 0.625 mm as described in section 2. The simulation of the gap was not possible due to its small dimension relative to the long extension of the geometry that would require a huge mesh. Simulations were performed to verify the effects of a similar gap on the pressure loss of a perforated plate with 81 orifices. A reduction of 4,7% of the pressure loss in these simulations was observed.

Other issue encountered was the presence of two 90 ° curves before the experimental test section as shown in Fig. 1. Simulations of this geometry, including the flow conditioner, confirmed that the velocity and turbulence profile is not appropriately developed at the entrance of the flow channel (just after the flow conditioner). Simulations applying the calculated profile to the BN were not possible due to large mesh requirements since the symmetry hypothesis is no longer valid. A reduction of about 4,5% in the pressure loss was observed in a simulation performed on a perforated plate with 81 orifices, in the position of the plate of the BN, in which the calculated non uniform profile was imposed at the entrance of the test section. The combination of these geometric and boundary condition effects together with the geometric simplifications applied to the BN could be responsible for most of the differences between numerical and experimental results. Further studies are necessary to evaluate the influence of gap, inlet profiles and geometric simplifications on the BN's simulation.

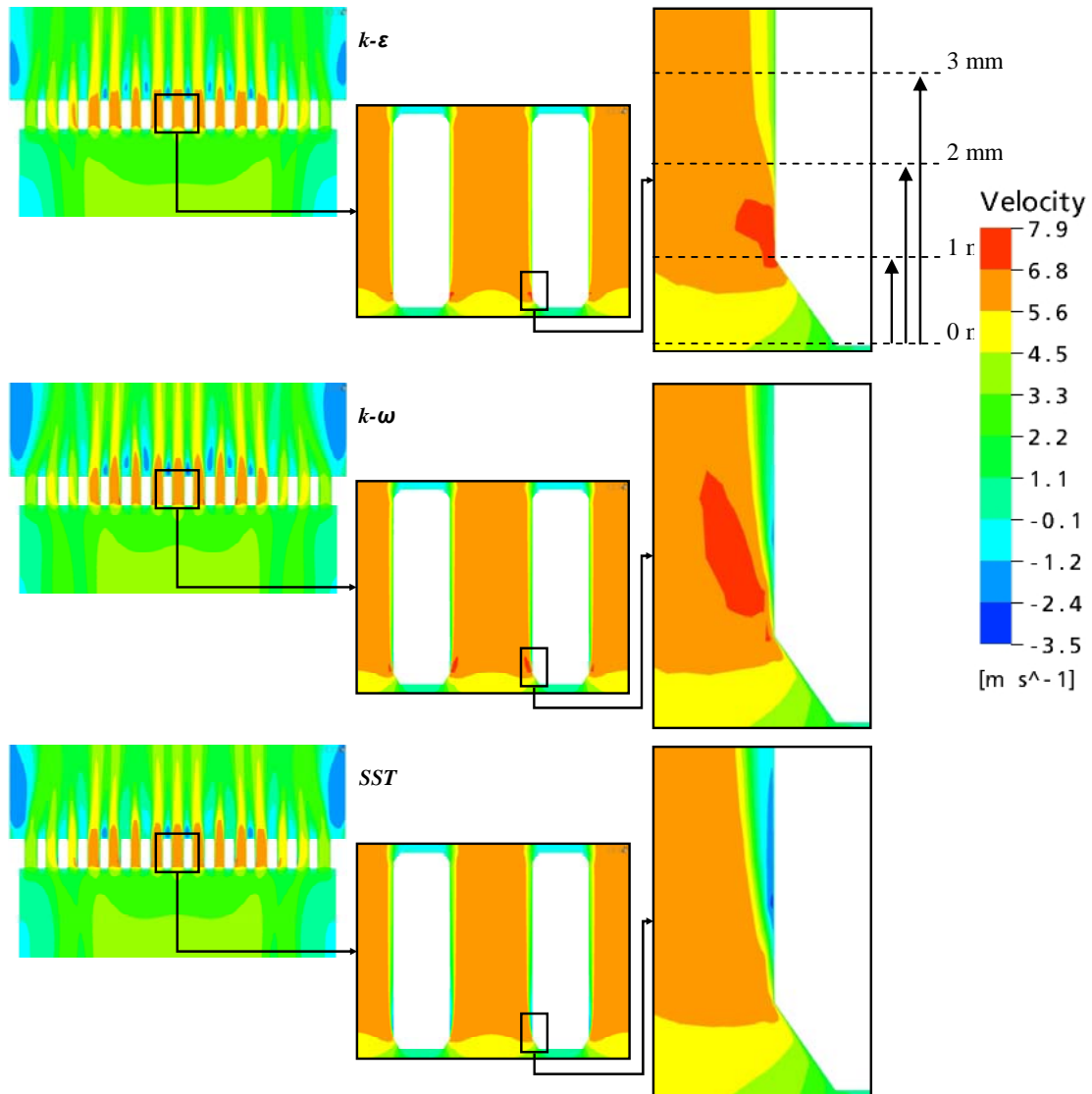


Figure 12. Velocity contours on the diagonal plane at the perforated plate region of the BN for three turbulence models.

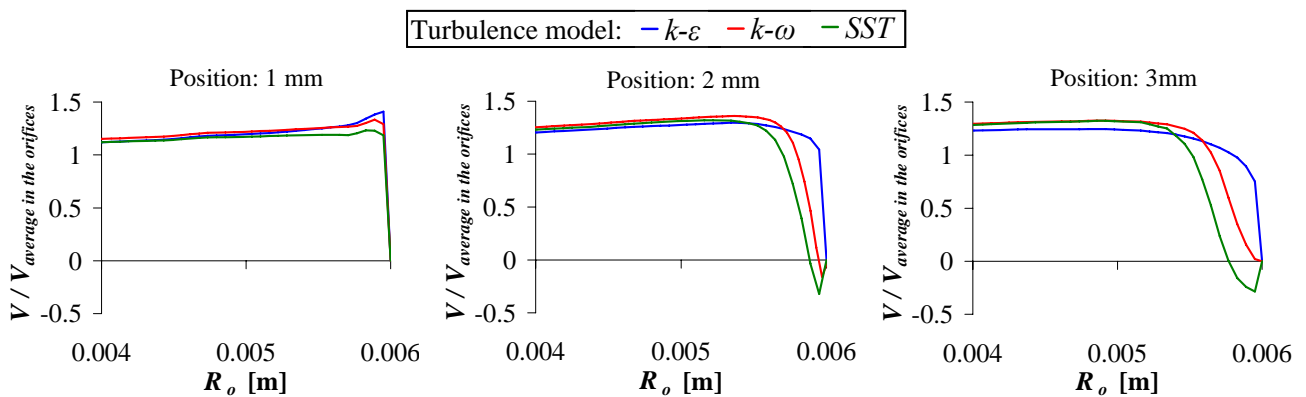


Figure 13. Near wall velocity profile at tree different positions (see Fig. 12) of the central orifice of the perforated plate of the BN for the simulated turbulence models.

5. CONCLUSION

In this analysis, experimental data concerning a pressure drop through a bottom end piece of a nuclear fuel element has been experimentally determined and compared to results from numerical simulations conducted with a commercial code CFX 10.0.

A mesh independence study was conducted splitting the BN in two separate geometries: the perforated plate and the bottom support. A large number of simulations were performed on both geometries applying different mesh configurations to obtain a mesh independent result. The $k-\varepsilon$ turbulence model was used in the simulations. Mesh controls were used to refine the superficial and volumetric mesh in specific regions of the BN to capture better the rapid flow contraction, expansion and recirculation.

The mesh parameters defined for the perforated plate and bottom support in the mesh independence study were applied to the BN where simulations were performed under the experimental flow condition applying $k-\varepsilon$, $k-\omega$ and SST RANS turbulence models.

Overall agreement between numerical results obtained with the $k-\varepsilon$ and SST turbulence models and experimental data can be considered satisfactory.

It was observed that most of the pressure loss on the flow through the BN is due to the perforated plate. The differences of predicted pressure loss on the perforated plate between the turbulence models were not altered downstream of the BN, thus, highlighting that it is critical to correctly predict the flow at this region.

Some simplifications were assumed in the geometric form of the piece which were responsible for some discrepancies obtained in the results. Limitations on the computational capacity disabled an appropriated simulation of the gap between the bottom end piece and the flow duct wall which can reach up to 0.625 mm and the use of velocity and turbulence profiles at the entrance of the flow channel. Further investigations are still necessary to evaluate influence of the gap and of the real inlet velocity and turbulence profiles on flow behavior.

Other turbulence models such as LES (Large Eddy Simulation) need to be appraised in the simulation of the BN.

6. ACKNOWLEDGEMENTS

The authors express their appreciation to the Centro Tecnológico da Marinha (CTMSP) and to the Indústrias Nucleares do Brasil (INB) for the experimental support to this research.

7. REFERENCES

- Anglart, H., Nylund, O., Kurul, N. and Podowski, M. Z., 1997, "CFD prediction of flow and phase distribution in fuel assemblies with spacers", Nuclear Engineering and Design, Vol. 177, pp. 215-228.
- Baglietto, E. and Ninokata, H., 2005, "A turbulence model study for simulating flow inside tight lattice rod bundles", Nuclear Engineering and Design, Vol. 235, pp. 773-784.
- Barth, T. J. and Jespersen, D. C., 1989, "The design and application of Upwind schemes on unstructured meshes", American Institute of Aeronautics and Astronautics Journal, Paper 89-0366.
- Campbell, R. L., Combala, J. M. and Hochreiter, L. E., 2005, "Computational fluid dynamics prediction of grid spacer thermal-hydraulic performance with comparison to experimental results", Nuclear Technology, Vol.149, pp. 49-61.
- CFX-10.0, 2005, "User manual", ANSYS-CFX.
- Frattolillo, A. and Massarotti, N., 2002, "Flow conditioners efficiency a comparison based on numerical approach", Flow Measurement and Instrumentation, Vol. 13, pp. 1-11.
- Házi, G., 2005, "On turbulence models for rod bundle flow computations", Annals of Nuclear Energy, Vol. 32, pp. 755-761.
- Ikeno, T., Kajishima, T. and Murata, T., 2006, "The effect of mixing-vane arrangements in a subchannel turbulent flow", Journal of Nuclear Science and Technology, Vol. 43, No. 10, pp. 1194-1205.
- Kolmogorov, A. N., 1942, "Equation of motion of an incompressible turbulent fluid", Izy. Akad Nauk SSSR Ser Phys VI, 56.
- Launder, B. E. and Spalding, D. B., 1974, "The numerical computation of turbulent flow", Computer Methods in Applied Mechanics and Energy, Vol. 3, pp. 269-289.
- Liu, R., Ting, D. S-K. and Rankin, 2004, "On the generation of turbulence with a perforated plate", Experimental Thermal and Fluid Science, Vol. 28, pp. 307-316.
- Menter, F. R., 1994, "Two-equation eddy-viscosity turbulence models for engineering applications", AIAA-Journal, 32, 269-289.
- Scheuerer, M., Heitsch, M., Menter, F., Egorov, Y., Toth, I., Bestion, D., Pigny, S., Paillere, H., Martin, A., Boucker, M., Krepper, E., Willemsen, S., Muhlbauer, P., Andeani, M., Smith, B., Karlsson, R., Henriksson, M., Hemstrom, B., Karpponen, I. and Kimber, G., 2005, "Evaluation of computational fluid dynamic methods for reactor safety analysis (ECORA)", Nuclear Engineering and Design, Vol. 235, pp. 359-368.
- Wilcox, D. C., 2000, "Turbulence modelling for CFD", DCW Industries, La Canada.

8. RESPONSIBILITY NOTICE

The authors are the only responsible for the printed material included in this paper.